

Universal Effectiveness of High-Depth Circuits in Variational Eigenproblems

Joonho Kim,^{1,*} Jaedeok Kim,^{2,*} and Dario Rosa^{3,4,*}

¹*School of Natural Sciences, Institute for Advanced Study, Princeton, NJ 08540, USA[†]*

²*AI Center, Samsung Research, Seoul 06765, Republic of Korea*

³*School of Physics, Korea Institute for Advanced Study,*

85 Hoegi-ro, Dongdaemun-gu, Seoul 02455, Republic of Korea

⁴*Department of Physics, Korea Advanced Institute of Science and Technology,
291 Daehak-ro, Yuseong-gu, Daejeon 34141, Republic of Korea*

We explore the effectiveness of high-depth, noiseless, parameteric quantum circuits by challenging their capability to simulate the ground states of quantum many-body Hamiltonians. Even a generic layered circuit Ansatz can approximate the ground state with high precision, as long as the circuit depth exceeds a certain threshold level that exponentially scales with the number of qubits, despite the abundance of the barren plateaus. This success is due to the fact that the energy landscape in the high-depth regime has a suitable structure for the gradient-based optimization, *i.e.* the presence of local extrema – near any random initial points – reaching the ground level energy. We check if these advantages are preserved across different Hamiltonians, by working out two variational eigensolver problems for the transverse field Ising model as well as for the Sachdev-Ye-Kitaev model. We expect that the contributing factors to the universal success of the high-depth circuits may also serve as the evaluation guidelines for more realistic circuit designs under hybrid quantum-classical algorithms.

I. INTRODUCTION

Variational Quantum Eigensolver (VQE) [1, 2] is one of the most promising hybrid quantum-classical (HQC) algorithms, which may offer a precise approximation of the ground state of quantum systems. It is based on the iterative application of the following three steps: state preparation, measurement and optimization. Let us briefly describe each step. First, the preparation of a trial wavefunction $|\psi(\theta)\rangle$ is carried out by successive application of unitary quantum gates that depend on variational parameters θ . Second, the measurement step estimates the trial state mean energy,

$$E(\theta) \equiv \langle \psi(\theta) | \mathcal{H} | \psi(\theta) \rangle, \quad (1)$$

by taking the expectation value of Hamiltonian \mathcal{H} of the target system over the trial state. Third, the optimization step adjusts the variational parameters θ of the trial wavefunction to minimize the mean state energy $E(\theta)$ by applying a classical optimization algorithm. See [3] and references therein for more details. After a sufficient number of iterations, the variational state $|\psi(\theta^*)\rangle$ at a convergence point $\theta = \theta^*$ is expected to reproduce well the ground state of the target Hamiltonian \mathcal{H} , under the assumption that the state Ansatz $|\psi(\theta)\rangle$ is *parametrically expressible* and *well-trainable* under the gradient based optimization. It is then a crucial question to find such an Ansatz.

We ideally expect that a generically successful Ansatz, which is capable of solving the VQE problem associated to an *arbitrary* target Hamiltonian, can closely approximate *any* random state $|\phi\rangle$ in the Hilbert space at specific

parameters. The existence of a parameter set φ , such that $|\psi(\varphi)\rangle \simeq |\phi\rangle$, is however not sufficient but merely necessary for universal effectiveness of the circuit. One also needs to look at whether or not the gradient descent optimization can actually reach the parameters φ . Although it may be sensitive to details of the optimization method, the overall trend is that generic layered circuits fit much better a random state when the number of layers exceeds a certain threshold value [4].

Concerning the usage of a generic layered circuit for the VQE algorithm, however, there has been a reported tension between increasing depth of layers and trainability of the circuit via the minimization of the mean energy, (1), known as the barren plateau phenomenon [5]. When the circuit reaches a certain depth such that it evolves to an approximate 2-design, a numerical experiment [5] has shown an exponential decay of the variance of energy function gradients $\nabla_{\theta} E(\theta)$ with the number of qubits — for states obtained by uniformly sampling from the parameter space. Combined with the vanishing mean of random gradients, as well as Chebyshev's inequality, it implies that the random gradient can exponentially rarely deviate from zero. Such vanishing gradients may make impossible an efficient optimization of generic layered circuits, causing the final variational state to stuck on sub-optimal plateaus.

Since then, various proposals have been made to overcome the vanishing gradient problem and efficiently simulate the ground state. The most obvious approach would be to incorporate some physical information and intuitions on the target Hamiltonian system [6–9], *e.g.* the ground state symmetry, to design a problem-tailored Ansatz which is less generic but can still express the desired state. However, since the physical understanding of a given Hamiltonian system is typically not readily available, it remains essential to improve the optimiza-

* All the authors contributed equally

[†] Correspondence to: joonhokim@ias.edu

tion performance of generic circuits — to make the applicability of the VQE algorithms *universal*, *i.e.* valid and trustworthy for generic Hamiltonians. Along this research direction, the novel initialization [10, 11], architecture [12, 13], and optimization [14–16] of generic purpose circuits have been invented and benchmarked, showing an improvement in performance. Interestingly, there are two seemingly conflicting claims about alternating layered circuits, *i.e.* circuits obtained by applying in sequence alternated layers of low-depth blocks. On the one hand, [12] has derived the *lower* bound of the variance of randomly sampled gradients, arguing that only low-depth circuits can avoid the barren plateau problem. On the other hand, [9] has observed a remarkable efficiency in optimizing high-depth circuits. The lesson we must take from these two examples is that the barren plateau phenomenon does not necessarily imply poor trainability of a given circuit under the gradient descent.

The main goal of this paper is to demonstrate the universal effectiveness of high-depth circuits in the *noiseless* VQE problems. To this end, we will show that, even though they undergo the barren plateau phenomenon, their trainability is hardly jeopardized under the VQE optimization for the following reasons:

First, although the magnitude $|\partial_i E(\theta)|$ of single gradient components becomes exponentially suppressed for the increasing number of qubits, the norm of the gradient vector $\|\nabla_\theta E(\theta)\|$ can grow to a finite size, capable of moving the initial state on the parameter space, if the circuit has sufficiently many layers and thus many parameters. It can be seen as a simple way to evade the main difficulties connected with the barren plateau phenomenon.

Second, the barren plateau phenomenon concerns only the initial steps of the VQE algorithm. We recall that the exponential suppression of the gradient components has been observed for *randomly* extracted values of the circuit parameters. In almost all physical systems of relevance, the Hamiltonian spectrum is symmetrically distributed around a certain value, which we canonically set to zero. A uniformly random choice of the parameters θ will then produce a state being a random superposition of multiple Hamiltonian eigenstates, whose mean energy (1) is highly likely to vanish, *i.e.* $E(\theta) \sim 0$. Once the VQE optimization starts up, however, the trial state quickly moves to smaller energies, where the variance of uniformly sampled gradients no longer is a relevant statistic.

Third, generically the VQE energy landscape $E(\theta)$ looks fairly simple in the vicinity of any randomly chosen point [16]. The random initial point is already confined in a certain basin of attraction, such that an associated optimization trajectory can quickly converge to a nearby local extremum. In particular, once the circuit has enough layers to become 2-design, almost all uniformly sampled initial states are rather homogeneous. The finally converged states after the VQE calculus are

also less variable, resulting in a similar energy level and local curvature in the parameter space.

Fourth, for high-depth circuits, all the local extrema in the energy landscape, reachable by the VQE optimization from randomly initialized points, tend to perform as good as the global minimum. This is the crucial feature being at the hearth of the robust success of the high-depth circuits in solving the VQE problems.

We will illustrate the above features of high-depth circuits by solving a concrete VQE problem for a very prototypical model of quantum many-body Hamiltonian: the 1d Ising model in a transverse, constant, magnetic field. Moreover, to show that these characteristics of the high-depth circuit are generic in the VQE setting, we will validate them by solving the Sachdev-Ye-Kitaev (SYK) model, which is a strongly interacting quantum mechanical system of Majorana fermions [17–19]. Despite the striking contrast in the quantum dynamics of these two Hamiltonians, the high-depth circuit shows a great performance for both models under the VQE algorithm. One may take it as an evidence of the universal effectiveness of the high-depth circuits.

Of course, the fundamental deficiency of the high-depth circuit is its infeasibility on the near-term quantum devices [20]. In particular, the problem of decoherence makes practically impossible to build a real high-depth quantum circuit. Nevertheless, our concrete motivation to examine the high-depth circuit is virtually twofold: Firstly, the high-depth circuit is an illustrative example to show that the occurrence of the barren plateau phenomenon does not necessarily hinder successful application of variational HQC methods [1, 2]. Secondly, some remarkable features of the high-depth circuit, which lead to its effectiveness under the VQE optimization, can serve as the operational guidelines for characterizing and evaluating more realistic circuit designs for a given problem that uses an HQC algorithm.

The rest of this paper is organized as follows. Section II introduces a particular type of the layered circuit Ansatz used throughout this paper, then estimates its parameteric expressibility for different numbers of layers. Section III studies the following aspects of the high-depth circuits: the occurrence of the barren plateau phenomenon, the loss curve, the optimization trajectory and energy landscape around a local extremum in the parameter space. We illustrate them using the VQE example of the 1d Ising model coupled to a uniform transverse magnetic field. Section IV considers another VQE problem for the SYK model, supporting the universal effectiveness of the high-depth circuit. Finally, Section V concludes with discussions.

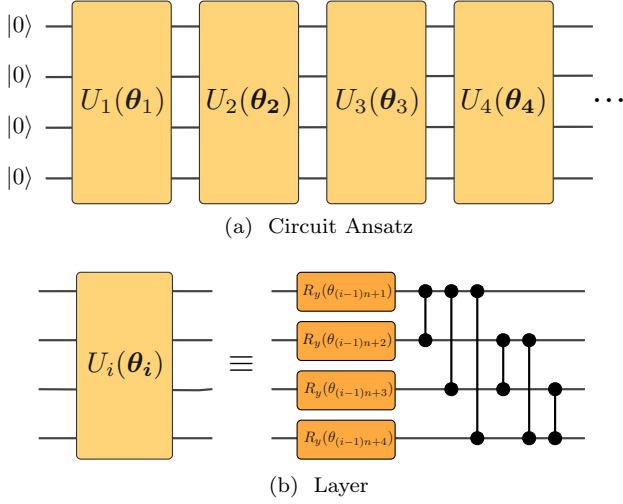


FIG. 1. The layered circuit Ansatz $|\psi(\theta)\rangle$ used in this paper.

II. CIRCUIT ANSATZES

Our primary focus in this work is to illustrate the efficiency of high-depth layered circuits in a typical VQE problem, *i.e.* to find the ground state of a given Hamiltonian. To this purpose, here we specify the architecture of the layered circuit ansatz adopted in our numerical experiments. The circuit state $|\psi(\theta)\rangle$ consists of L alternating layers acting on the initial state $|0\rangle$, *i.e.*,

$$|\psi(\theta)\rangle = U_L(\theta_L) U_{L-1}(\theta_{L-1}) \cdots U_2(\theta_2) U_1(\theta_1) |0\rangle, \quad (2)$$

where each layer $U_i(\theta_i)$ has single-qubit y -rotation gates, parameterized by n periodic variables θ_i , and controlled- z gates operating on all pairs of n qubits. More precisely, once the single-qubit RY gates have acted upon all individual qubits, the entangling CZ gates acting on a -th controlling and b -th targeting qubits are arranged for every integer pair (a, b) satisfying $1 \leq a < b \leq n$ [15]. An illustration of the circuit state (2) for the case with $n = 4$ qubits is given in Figure 1.

It should be stressed that we have deliberately chosen the rather generic circuit design as of [5, 12, 15], not particularly making use of physical properties of the system under investigation. Nonetheless, in Sections III and IV, we will see that the above circuit performs well for the VQE problems with different target Hamiltonians, as long as the number L of layers is sufficiently large, thus showing the universal effectiveness of the high-depth circuit [4, 9].

1. Parametric Expressibility

To start with, let us evaluate the circuit's capability to approximate closely random states, denoted by $|\phi\rangle$, with an appropriate choice of the circuit parameters θ .

Our variational circuit $|\psi(\theta)\rangle$ of L layers depends on nL parameters, $\theta = \{\theta_{(i-1)n+a} \mid 1 \leq i \leq L \text{ and } 1 \leq a \leq n\}$, which are periodic over the finite interval $[0, 2\pi)$ up to an overall sign. In other words, the Ansatz (2) defines a mapping from the nL -dimensional torus to the Hilbert space of n qubits. Such a map is called to be a t -design if the statistical distribution of the circuit states mimics the distribution of the Haar random states up to the t 'th-order moments [21]. For verification of their t -designness, it is required to compute the t 'th frame potential of the Ansatz state distribution,

$$\mathcal{F}^{(t)} = \int d\theta \int d\varphi |\langle \psi(\theta) | \psi(\varphi) \rangle|^{2t}, \quad (3)$$

and check if it saturates the lower bound of the inequality,

$$\mathcal{F}^{(t)} \geq \mathcal{F}_{\text{Haar}}^{(t)} = \frac{t!(2^n - 1)!}{(t + 2^n - 1)!}, \quad (4)$$

which is the t 'th frame potential of the Haar state distribution [22–24]. However, the Monte Carlo integration of (3) can be computationally demanding due to the need for collecting exponentially many samples with respect to the number of qubits n and layers L , also known as the curse of dimensionality.

Instead, as a more practical measure of the capability of simulating random states in the HQC algorithms, we find it useful to examine if, for any given Haar random state $|\phi\rangle$, there exist a point θ^* in the parameter space, reachable by the gradient-based optimization, at which $|\psi(\theta^*)\rangle \simeq |\phi\rangle$. This notion of expressibility, tailored for HQC approaches, can be estimated as follows: let us apply the gradient descent to find the minimum distance at the closest point

$$\theta^* = \arg \min_{\theta} \| |\psi(\theta)\rangle - |\phi\rangle \| \quad (5)$$

between the circuit and target states, where $\|\cdot\|$ is the Euclidean norm of a complex vector. The parametric (in)expressibility of the circuit $|\psi(\theta)\rangle$ is then defined as the minimum distance averaged over Haar random states:

$$\varepsilon = \frac{1}{\text{Vol}(U(2^n))} \int d\mu_{\phi} \min_{\theta} \| |\psi(\theta)\rangle - |\phi\rangle \|. \quad (6)$$

Notice that the closeness between two quantum states is usually defined by using the fidelity or the trace distance. Instead, we have adopted the Euclidean distance to improve the convexity of the optimization landscape, such that the closest point θ^* can be found as easily as possible, trying to untangle the notion of the parametric (in)expressibility from actual geometric obstacles in applying HQC algorithms [5, 12]. Indeed, the Euclidean norm defines trivially a convex space. Hence, the possible non-convexity in the optimization landscape is just inherited from the embedding of the nL -dimensional torus into the Hilbert space.

For the actual benchmark of the layered circuit's parametric expressibility, with different numbers L of layers,

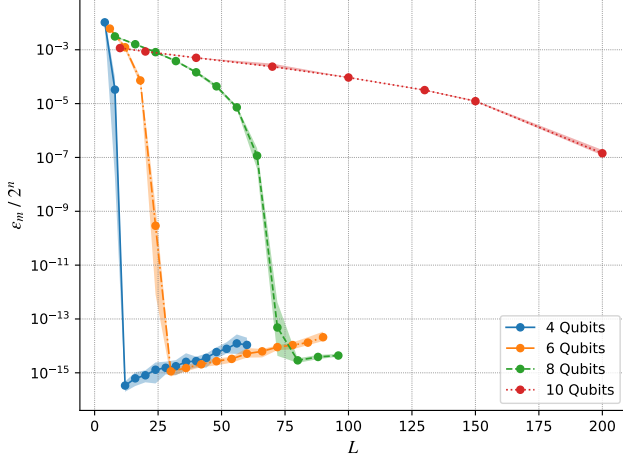


FIG. 2. The parametric (in)expressibility of the layered circuit Ansatz over $m = 10$ random target samples, $\varepsilon_{m=10}/2^n$, normalized by the number 2^n of state components. The narrow shade denotes the fluctuation across $m = 10$ target states.

it is more convenient to substitute the Haar integral (6) with the sample mean over m Haar random states:

$$\varepsilon_m = \frac{1}{m} \sum_{i=1}^m \min_{\theta} \|\psi(\theta)\rangle - |\phi_i\rangle\| \quad (7)$$

Given a random target state $|\phi_i\rangle$, we start with an Ansatz state $|\psi(\theta)\rangle$ with nL initial parameters θ , randomly sampled from the product uniform distribution $\mathcal{U}(0, 2\pi)^{\otimes nL}$. To reach the optimal parameters θ^* that minimize the distance, we apply the Adam optimization algorithm [25], which iteratively updates the variational parameters θ by the exponential moving averages of gradients and their squares. It has a clear advantage in convergence speed, being widely used in a variety of deep learning models such as recurrent networks [26, 27], convolution networks [28], and graph networks [29]. The parameter update rule is concretely determined by a choice of the hyperparameters $(\alpha, \beta_1, \beta_2)$ defined in [25]. In the current benchmark, we have specifically used the learning rate $\alpha = 0.05$ and the exponential decay rates $\beta_1 = 0.9$ and $\beta_2 = 0.999$ for the moving averages.

Figure 2 shows the sample mean ε_m over $m = 10$ random target states, divided by the number 2^n of state components. The narrow shade displays the fluctuation range of the component-averaged distance $\|\psi(\theta^*)\rangle - |\phi_i\rangle\| \cdot 2^{-n}$ across different target states indexed by $i = 1, \dots, 10$. We have selected the minimum distance among the first $\tau \leq 500$ optimization steps, which is sufficient since the optimal parameter θ^* is empirically always found in an early stage of the optimization.

We observe that parametric (in)expressibility regularly converges to 0 as the circuit depth L grows. In particular, it approaches to 0 with high precision, *i.e.*,

$$\varepsilon_{m=10} \leq 10^{-5} \cdot 2^n, \quad (8)$$

when the depth L is greater than the following threshold values:

n qubits	4	6	8	10
L_ε layers	10	24	56	150

Note that a slight ramp-up follows after the sudden collapse of $\varepsilon_{m=10}$, caused by the random walk of the circuit parameter θ around the optimal point θ^* , since the random step size gets amplified for bigger L . Such fluctuation is a common phenomenon in gradient-based optimization, where a suitable reduction of the learning rate may supersede it to the stable convergence $\theta \rightarrow \theta^*$. For instance, at the learning rate $\alpha = 0.01$, the 6-qubit circuit $|\psi(\theta)\rangle$ with $L = 90$ layers achieves $\varepsilon_{m=10} < 10^{-15} \cdot 2^6$, which is roughly the same as of $L = 24$ layers.

By evaluating the layered circuit Ansatz (2) of variable depths, based on their parametric (in)expressibility ε , we have clearly observed the following trend: Deeper circuits are not only a superset of shallow circuits but also behave more effectively in the gradient-based optimization. It should be taken as a preliminary evidence exhibiting the effectiveness of deep circuits. One may further ask if the high-depth circuit is generally well-trainable under variational HQC problems, *i.e.* in which the intrinsic convexity of the Euclidean norm is lost and, moreover, in which the state to be approximated is rather *non-generic*, being the ground state of quantum many-body Hamiltonian. We will see in the next section that the high-depth circuits can indeed approximate well the ground state of the target Hamiltonian \mathcal{H} in typical VQE problems.

III. LOOKING INTO VQE TRAJECTORIES

This section is devoted to the detailed investigation of the VQE optimization procedure, with a particular focus on the effectiveness of the high-depth circuit Ansatz (2). Our exploration will be based on a concrete Hamiltonian system, commonly used in measuring the performance of variational circuits, *i.e.* the 1d Ising model in a transverse and uniform magnetic field [9, 30].

The 1d transverse field Ising model is defined over a spin lattice of length n , consisting of the spin-spin coupling between nearest neighbors in the z direction, as well as the spin interaction with a background uniform magnetic field along the transverse x direction. Assuming periodic boundary conditions, $\sigma_{n+1}^z \equiv \sigma_1^z$, the ferromagnetic Ising Hamiltonian reads

$$\mathcal{H} \equiv - \sum_{i=1}^n \sigma_i^z \sigma_{i+1}^z - g \sum_i \sigma_i^x, \quad (9)$$

where $\sigma_i^{x,y,z}$ is the Pauli operator acting on the i 'th spin, and g denotes the strength of the uniform magnetic field.

The physics of this model has been well-studied [31]. When the lattice size scales up to infinity, $n \rightarrow \infty$, the

system undergoes a *quantum* phase transition at $|g| = 1$ between the ordered ($|g| < 1$) and disordered ($|g| > 1$) phases. The former phase has the spin-flip \mathbb{Z}_2 symmetry that connects the two opposite ferromagnetic ground states, while the latter phase has a unique ground state, with all the spins aligned along the x direction.

We will apply the VQE algorithm to the finite n Ising system, which exhibits some differences from the thermodynamic limit. Specifically, the \mathbb{Z}_2 degeneracy in the $0 < |g| < 1$ phase is broken at finite n . Our target state will be then always non-degenerate and will have a small energy gap with the next excited state for any $|g| \neq 0$. All concrete calculations presented in this section have been done for $g = 2$.

1. Barren Plateau Phenomena

It has been argued that the abundance of the barren plateaus can be the most fundamental obstacle in optimizing a randomly initialized variational circuits [5]. The essence is that for generic 2-design circuits, random initial points are highly likely located at plateaus in the energy landscape, such that the gradient-based optimization algorithm cannot start. The probability of having non-vanishing gradients at random points decays exponentially with the number n of qubits, thus creating a concern for scaling up the system size. Its effect can be even more detrimental to the trainability of generic variational circuits on actual quantum devices, where the presence of noise, under the form of sampling errors, must be taken into account. Accurate computation of a gradient which decays exponentially with the system size n demands exponentially many samples, eliminating the scaling advantage of quantum machines [5, 15]. Given the prominence of this phenomenon, we begin by reviewing the barren plateau phenomenon in the VQE problem.

Let us collect the energy gradient at every point in the nL -dimensional torus, $[0, 2\pi)^{\otimes nL}$, for the VQE problem with the layered circuit (2) and target Hamiltonian (9). To analyze the k 'th partial derivative, $\partial_k E(\theta)$, with respect to the angle θ_k that belongs to the ℓ 'th variational layer, it is convenient to decompose the state Ansatz (2) into two blocks [5]

$$|\psi(\theta)\rangle = U_-(\theta_-) U_+(\theta_+) |0\rangle, \quad (10)$$

where $\theta_q = \{\theta_p \mid \lfloor \frac{p}{n} \rfloor = q\}$, $\theta_+ = \bigcup_{a \leq \ell} \theta_a$, $\theta_- = \bigcup_{a > \ell} \theta_a$,

$$\begin{aligned} U_+(\theta_+) &\equiv U_\ell(\theta_\ell) U_{\ell-1}(\theta_{\ell-1}) \cdots U_2(\theta_2) U_1(\theta_1), \\ U_-(\theta_-) &\equiv U_L(\theta_L) \cdots U_{\ell+2}(\theta_{\ell+2}) U_{\ell+1}(\theta_{\ell+1}). \end{aligned} \quad (11)$$

As the partial derivative ∂_k acts only on $U_\ell(\theta_\ell)$, the variance of the k 'th gradient component, $\text{Var}_\theta[\partial_k E(\theta)]$, is

$$-\int \frac{d\theta}{(2\pi)^{nL}} \langle \psi(\theta) | [U_-(\theta_-) V_k U_-(\theta_-)^\dagger, \mathcal{H}] | \psi(\theta) \rangle^2 \quad (12)$$

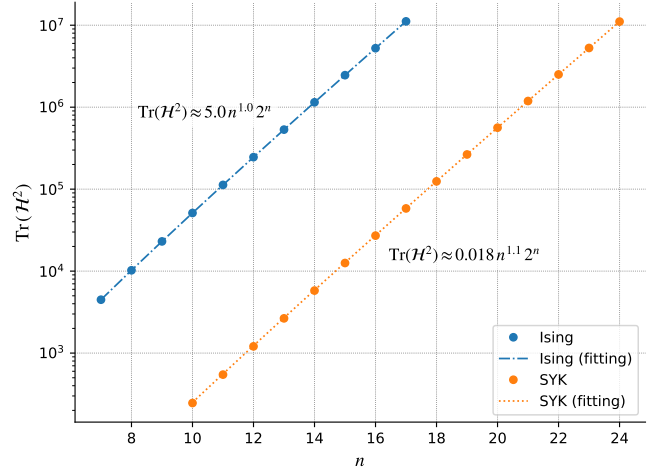


FIG. 3. $\text{Tr}(\mathcal{H}^2)$ of the Ising model (9) and the SYK model (26) as a function of the system size n . The dashed lines are the regression lines with the functional form of $a \cdot n^b 2^n$, based on the numerical data denoted as small circles.

where V_k denotes the Pauli operator σ_i^y acting on the k 'th spin variable, such that $\text{Tr}(V_k) = 0$ and $\text{Tr}(V_k^2) = 2^n$.

If we further assume the 2-design property of $U_+(\theta_+)$ and/or $U_-(\theta_-)$, the above integral (12) can be replaced with the unitary matrix integral. In that case, the matrix integral can be handled exactly and simplified to [5, 12]

$$\frac{2\text{Tr}(\mathcal{H}^2)}{2^{2n}}. \quad (13)$$

Such simplification (13) happens when both $U_\pm(\theta_\pm)$ are 2-designs. Instead, if the 2-design condition does not hold for either of $U_\pm(\theta_\pm)$, we have the following expression:

$$-\frac{1}{2^{2n}} \int \frac{d\theta_-}{(2\pi)^{n(L-\ell)}} \text{Tr}([V_k, U_-(\theta_-)^\dagger \mathcal{H} U_-(\theta_-)]^2) \quad (14)$$

if only $U_+(\theta_+)$ is a 2-design while $U_-(\theta_-)$ is not, or

$$-\frac{\text{Tr}(\mathcal{H}^2)}{2^{2n}} \int \frac{d\theta_+}{(2\pi)^{n\ell}} \text{Tr}([V_k, U_+(\theta_+)^\dagger \rho U_+(\theta_+)]^2) \quad (15)$$

where $\rho = |0\rangle\langle 0|$, if not $U_+(\theta_+)$ but only $U_-(\theta_-)$ is a 2-design. These asymptotic expressions (13)–(15) are all bounded as

$$0 \leq \text{Var}_\theta[\partial_k E(\theta)] \leq \frac{4\text{Tr}(\mathcal{H}^2)}{2^{2n}}, \quad (16)$$

where the upper bound is obtained by expanding the commutator inside the integral of (14) and (15), then making use of the following trace inequality that holds for two Hermitian matrices A, B [32]:

$$|\text{Tr}(AB)^{2m}| \leq \text{Tr}(A^{2m} B^{2m}) \quad \text{for } m \in \mathbb{N}. \quad (17)$$

To determine the scaling behavior of the upper bound (16) with respect to the system size n , we have examined

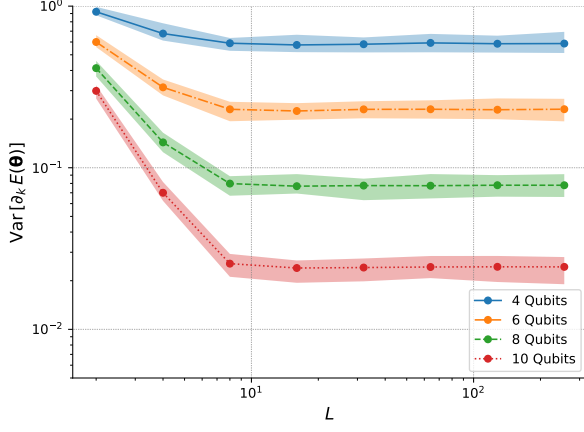
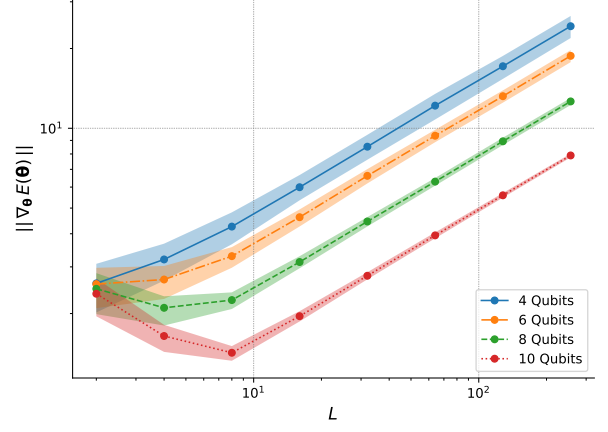
(a) Sample variance of the energy derivative $\partial_k E(\theta)$ (b) Sample average of the Euclidean norm of $\nabla_\theta E(\theta)$

FIG. 4. The barren plateau experiment for the Ising Hamiltonian (9). The shades indicate (a) the variance across gradient components $\{\partial_k E(\theta)\}_{k=1}^{nL}$, (b) the first and third sample quantiles.

how $\text{Tr}(\mathcal{H}^2)$ scales with n by extrapolating the values obtained from exact diagonalization of (9) up to $n \leq 17$. The results are presented in Figure 3. We see that the term $\text{Tr}(\mathcal{H}^2)$ scales as 2^n , such that the exponential factor in the denominator of the upper bound (16) cannot fully be balanced by $\text{Tr}(\mathcal{H}^2)$. Then, inserting the upper bound (16) to Chebyshev's inequality, which states

$$\Pr(|\partial_k E(\theta)| > \epsilon) < \frac{\text{Var}_\theta[\partial_k E(\theta)]}{\epsilon^2} \quad (18)$$

with $\partial_k E(\theta)$ being a random variable of mean 0, the probability of having a non-zero and finite energy derivative is exponentially suppressed with growing n . Therefore, the occurrence of the barren plateau phenomenon is expected for the VQE problem with the Ising model (9).

So far, the argument has been based on the assumption that at least one of the unitaries $U_\pm(\theta_\pm)$ is a 2-design, which is a characteristic that has not been tested. Hence, to confirm the previous results, we now turn to examine numerically if our circuit state (2) is sufficiently random to create the barren plateaus in the associated VQE landscapes. Treating the gradient of the VQE energy function $\partial_k E(\theta)$ as random variables, we have calculated their sample variance over a random collection of 1000 parameters. Figure 4a clearly exhibits the exponential decay of each component of the gradient vector with increasing number n of qubits, where the shaded region displays component-wise fluctuations of the variance, $\text{Var}_\theta[\partial_k E(\theta)]$, for all $1 \leq k \leq nL$. These results confirm that our specific VQE landscapes indeed contain the barren plateaus, which could possibly interfere the gradient-descent based optimization of the variational circuit (2) [5, 12, 15].

On the other hand, Figure 4a shows that the variance, at a fixed value of n , converges to a constant by increasing the number L of layers, *i.e.* it is independent of L

after a transition point L_0 where the circuit Ansatz (2) with $L \geq L_0$ layers evolves to 2-design [5]. It means that the vanishing gradient problem can be circumvented in a straightforward manner, *i.e.* by accumulating an adequate number of layers. Due to the saturation of the variance, adding exponentially many layers can always compensate for the exponential decay of each component value when calculating the gradient norm $\|\nabla_\theta E(\theta)\|$, which appears in the dynamics of the VQE mean energy under the vanilla gradient descent with the learning rate α :

$$\frac{dE(\theta)}{d\tau} = -\alpha \|\nabla_\theta E(\theta)\|^2 \quad (19)$$

Such gradient configuration behaves as a finite-sized vector in an exponentially large space, with each components being exponentially suppressed. In agreement with the reasoning above, Figure 4b exhibits a small initial drop, dominated by the transient decrease of $\text{Var}_\theta[\partial_k E(\theta)]$ for $L \leq L_0$ layers, followed by a steady increase, driven by the growth in the number nL of the gradient components. One can estimate the increase rate of the norm $\|\nabla_\theta E(\theta)\|$ as

$$\|\nabla_\theta E(\theta)\| \sim \sqrt{nL \times \text{Var}_\theta[\partial_k E(\theta)]} \quad (20)$$

which agrees well with the empirically measured growth rates between $\log \|\nabla_\theta E(\theta)\|$ and $\log L$ in Figure 4b:

n qubits	4	6	8	10
rate	0.504	0.502	0.503	0.501

Having found that the fading gradient problem can be trivially avoided at the cost of introducing exponentially many layers, we turn to answer if the variational circuit (2) with a sufficiently many layers can actually solve the VQE problems. We will examine the minimum optimization error, the training curve, as well as the trajectory in the parameter space for different numbers of layers.

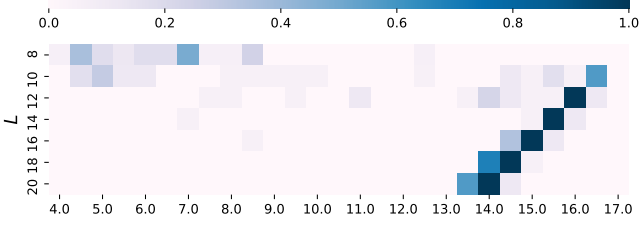


FIG. 5. Optimized VQE energy ($E(\theta^*) - E_0$) density for the Ising model over 35 distinct runs with random initialization.

2. Optimizing the Circuit

The VQE optimization result of the circuit states (2), with different numbers L of layers and under the random initialization of the circuit parameters θ , can be summarized to the following two aspects:

1. For random initial states $|\psi(\theta)\rangle$ with small enough L , the circuit parameter θ converges to a local extremum θ^* with highly variable VQE energy $E(\theta^*)$.
2. For larger L , the $E(\theta^*)$ distribution turns sharply concentrated around a mean value which gets smaller.

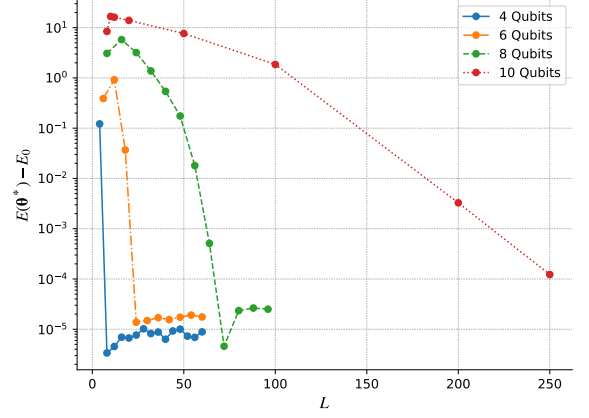
Let us illustrate these points with the 10-qubit outcomes of the VQE algorithm for $L \in \{8, 10, 12, 14, 16, 18, 20\}$. We have collected 35 independent VQE runs for the Ising Hamiltonian (9), whose initial parameters are randomly sampled from the uniform distribution $\mathcal{U}(0, 2\pi)^{\otimes nL}$, after 500 parameter updates with Adam optimizer [25] and the hyperparameters $(\alpha, \beta_1, \beta_2) = (0.05, 0.9, 0.999)$.

The sample distribution of the final VQE energy $E(\theta^*)$ is visualized in Figure 5 for different numbers L of layers. One can characterize it as follows. First, the energy distribution at the local extremum θ^* clearly exhibits the widespread spectrum for a shallow depth, *e.g.*,

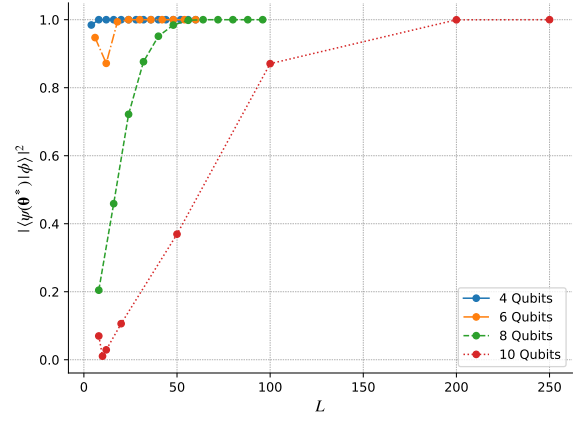
$$\begin{aligned} 3.52 \leq E(\theta^*) - E_0 \leq 12.6 & \quad \text{for } L = 8, \\ 4.67 \leq E(\theta^*) - E_0 \leq 16.9 & \quad \text{for } L = 10, \end{aligned}$$

sometimes achieving a relatively good energy level, given their limited degree of the parametric expressibility (6). Such variability shows that the circuit is still shallow, not having evolved yet to a random 2-design, being consistent with Figure 4a. Second, by stacking more layers, *i.e.*, $L \geq 12$, deeper than the 2-design transition point detected in Figure 4a, the energy distribution starts to concentrate around a single value, which is farther from the ground state energy E_0 . Third, the average value of $E(\theta^*)$ continues to decrease for the growing number L of layers, suggesting that high-depth variational circuits may be able to reach the ground state by means of the VQE optimization.

Encouraged by the observed shrinkage of the mean and variance of $E(\theta^*)$, we also have done the single VQE



(a) The VQE optimization error $E(\theta^*) - E_0$



(b) Fidelity between the optimized and true ground states

FIG. 6. Single-run VQE outcomes for the Ising model (9) using the layered circuit Ansatz (2) at different depths L .

tryouts for a broader span of (n, L) , as summarized in Figure 6. It is evident that the deep circuits make it easy to replicate a true ground state $|\psi_0\rangle$, reaching the ground energy level E_0 and achieving high values of fidelity with $|\psi_0\rangle$. The overall characteristics of Figure 6a is similar to Figure 2, achieving a zero error with the following precision:

$$|E(\theta) - E_0| \leq 10^{-5} \cdot \Delta E \quad (21)$$

where ΔE denotes the bandwidth of the target Hamiltonian \mathcal{H} , defined as the difference between the largest eigenvalue of \mathcal{H} and the ground state energy, E_0 . We note that such precision can be achieved only with an appropriately chosen learning rate α , in order to avoid too-large parameter updates that prevent the fine-level optimization. Here we refrain from the systematic hyperparameter search, which may be more relevant for the case where the average gap between nearby energy levels shrinks, but simply stick to $\alpha = 0.05$ ($L = 4, 6, 8$) and $\alpha = 0.01$ ($L = 10$). We have found that (21) can be achieved when the circuit depth L passes through the

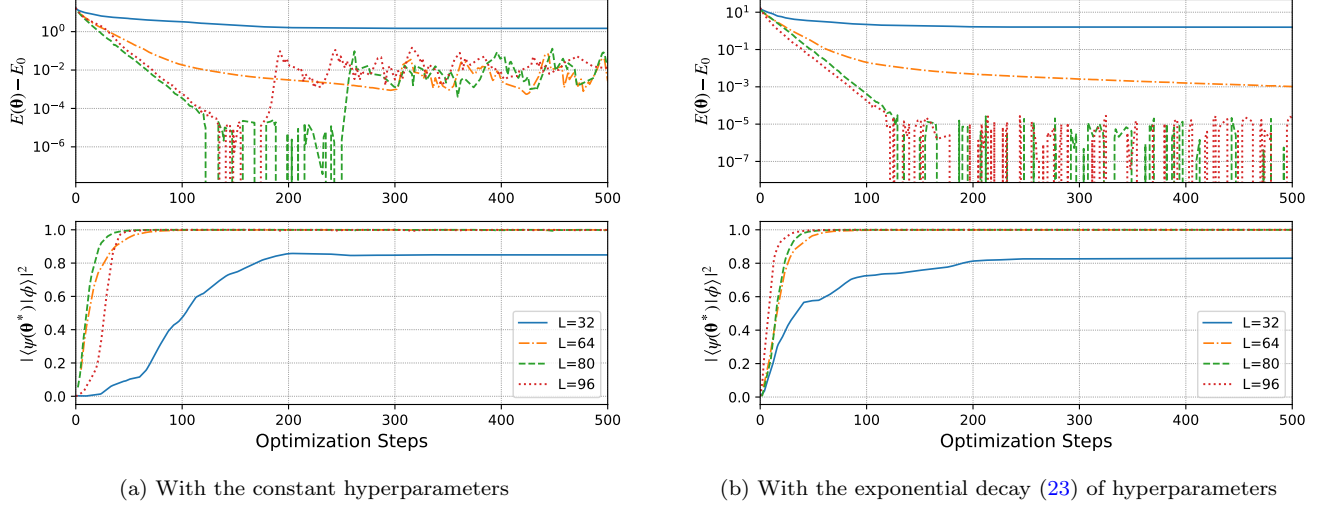


FIG. 7. Optimization curves of the circuit state on the Ising model at 8 qubits. The upper and lower plots denote the VQE error $E(\theta_\tau) - E_0$ and the fidelity $|\langle \psi(\theta^*) | \phi \rangle|^2$ between the circuit and true ground states, respectively, as a function of the optimization steps τ . Notice the late-time fluctuation has been alleviated with the learning rate scheduling.

following threshold value:

n qubits	4	6	8	10
L_v layers	10	24	68	250

We also remark that deeper circuits do not necessarily lead to better performance with VQE, as displayed by the gentle ramp after passing the threshold point L_v . This can be understood as follows: As the space of variational parameters θ has more dimensions, the basin of attractor to local extrema becomes narrower [12], giving a larger value of the estimated inverse volume [33]

$$V_k^{-1} = \sum_{i=1}^k \log \lambda_i(H) \quad (22)$$

where the summation is taken over the top- k eigenvalues $\{\lambda_i(H)\}_{i=1}^k$ of the Hessian matrix $H_{ij} \equiv \partial_i \partial_j E(\theta)$. For instance, the positive correlation between L and $V_k^{-1}(L)$ can clearly be identified in Figure 8a, drawn for $k = 100$. As a result, the VQE trajectory is unlikely to land at an exact extremum but wander around nearby points, whose deviation gets larger as the attractor basin becomes narrower and steeper.

Even with the optimal number of layers, such that the circuit state can reach an exact extremum and accurately represent the ground state $|\psi_0\rangle$ of the Ising Hamiltonian (9), the narrowness of the attractor basin still makes the VQE trajectory somewhat unstoppable, passing through the best point θ^* and then hopping around in the local neighborhood. Figure 7a shows that the VQE error $E(\theta_\tau) - E_0$ slightly increases on average and mildly fluctuates after achieving the minimum error $E(\theta^*) - E_0$. This residual error can be reduced by making use of popular optimization tricks, such as early stopping or learning rate scheduling, which causes the VQE optimization

to stop at the optimal point. For instance, by introducing the exponential decay of the learning rate α , *i.e.*

$$\alpha_\tau = \alpha_0 c^{\tau/500}, \quad \tau \geq 0 \quad (23)$$

at the optimization step τ with a constant value $c = 0.3$, we could reduce the late time fluctuations as in Figure 7b.

So far we have discussed some generic aspects of the VQE optimization. The main message is that, contrary to the common belief, randomly initialized deep circuits can achieve higher performance than their shallow counterparts. Along the optimization trajectory, the gradient flow neither disappears nor randomly fluctuates, so that the circuit (2) can easily converge to a local minimum, showing a small energy gap from the ground energy E_0 and high fidelity with the exact ground state $|\psi_0\rangle$. We will explore this efficiency of the high-depth circuit in some details by visualizing the VQE trajectory on the energy landscape.

3. Visualizing the Trajectory

A remarkable characteristic that mainly contributes to the generic success of the high-depth circuit is the fact that randomly initialized points are likely to be already confined in the basin of attraction of a good attractor, *i.e.* a local extremum with a small enough value of the energy. We illustrate now this point by looking at the actual optimization trajectories under the VQE algorithm.

For a given initial point θ_0 and the trajectory $\mathcal{T}(\theta_0) = \{\theta_\tau\}$ thereafter, we identify the optimal parameter θ^* as the point in the trajectory $\mathcal{T}(\theta_0)$ having the minimum

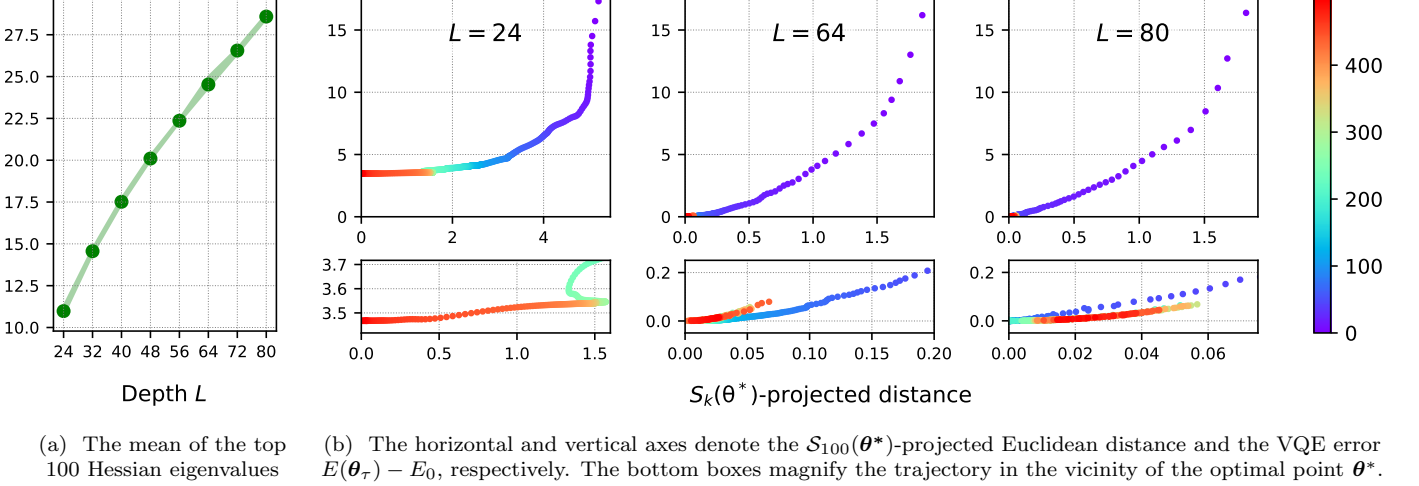


FIG. 8. The visualization of the optimization trajectory in the 100 steepest directions for the Ising model with $n = 8$ qubits.

energy expectation value,

$$E(\theta^*) \leq E(\theta_\tau) \quad \text{for any } \tau \geq 0, \quad (24)$$

which is the best possible representative point of the local extrema that the trajectory $\mathcal{T}(\theta_0)$ converges around. The associated basin of attractor can be estimated by calculating the Hessian $H_{ij} \equiv \partial_i \partial_j E(\theta^*)$ at the optimum θ^* . We are interested in the eigenvalue spectrum, $\{\lambda_i(H)\}$, from which we distinguish steep and flat directions and estimate the degree of steepness.

Similar to the case of deep neural networks [33–35], the local extrema in the VQE energy landscape of high-depth circuits are often interconnected in multiple flat directions, whose corresponding Hessian eigenvalues are zero, looking like valleys rather than isolated singular points. Success of the VQE algorithm is not affected by a specific position in flat directions, but only concerned with if a ball, initially at a considerable height, can roll off in steep directions and reach a sufficiently deep gorge. It motivates us to consider the k -dimensional hypersurface $\mathcal{S}_k(\theta^*)$ along the k steepest directions, *i.e.*, spanned by the top- k Hessian eigenvectors [33]. More precisely, we want to examine if the $\mathcal{S}_k(\theta^*)$ -projected Euclidean distance between θ^* and θ_τ decreases along the trajectory $\mathcal{T}(\theta_0)$ as the optimization step τ progresses, until $E(\theta_\tau) = E(\theta^*)$. This will tell us if the entire trajectory $\mathcal{T}(\theta_0)$ is confined in the k -dimensional basin of attraction, while ignoring the movement in the directions of less or zero attraction.

Figure 8b displays the VQE error $E(\theta_\tau) - E_0$ and the projection distance $\|\theta_\tau - \theta^*\|_{\mathcal{S}_{100}(\theta^*)}$ along the actual optimization trajectories, whose step number τ is indicated by color. We have made the following observations: First, when an appropriate value of k is selected, both the distance $\|\theta_\tau - \theta^*\|_{\mathcal{S}_k(\theta^*)}$ and the loss value $E(\theta_\tau) - E_0$ continuously decrease on a macroscopic scale. It exhibits that the trajectory $\mathcal{T}(\theta_0)$ converges without escaping

from a specific basin of the attractor that encloses a randomly initialized point θ_0 . Second, for a shallow circuit state, the optimization trajectory often makes a slight detour in some orthogonal directions. In contrast, the steady convergence occurs typically for large L . It implies that the vicinity of any randomly initialized parameters is effectively convex. Finally, we find from Figure 8a that the attractor basin in the direction of $\mathcal{S}_k(\theta^*)$ evolves rapidly steeper and narrower as the depth L increases, thereby causing the rapid convergence and substantial late-time fluctuation around θ^* . It is noticeable that the initial convergence follows a milder path than later fluctuations in the $L = 64$ case, while the convergence in the $L = 80$ case happens along a much steeper route. Taken together, these observations show the quick convergence of high-depth circuits under the VQE optimization [4, 9].

IV. SOLVING THE SYK MODEL

Our discussions so far have been based on just a particular Hamiltonian (9), the Ising model in a transverse uniform magnetic field. As already emphasized, the layered circuit Ansatz (2) is rather generic and has no features particularly tailored for the Ising model. We thus expect that the high-depth circuits should be equally successful in other VQE problems solving different quantum Hamiltonians. To check the generality of our prior discussions on the efficiency of the high-depth circuits, we will now analyze the VQE problem, defined for another Hamiltonian of very distinct nature: the SYK model.

1. The SYK Model

The SYK model [17–19] is built out of $2n$ Majorana fermions in $1d$, *i.e.* the operators γ_i , with $i = 1, \dots, 2n$, satisfying the following anti-commutation relations

$$\{\gamma_i, \gamma_j\} = \delta_{ij}, \quad (25)$$

where δ_{ij} denotes the Kronecker delta. The SYK Hamiltonian is an all-to-all Hamiltonian, which couples all the Majorana fermions together in a fully non-local fashion, consisting of the following q -body interaction terms with $q \geq 2$ being an even integer:

$$\mathcal{H} \equiv (i)^{q/2} \sum_{i_1 < \dots < i_q} J_{i_1 \dots i_q} \gamma_{i_1} \cdots \gamma_{i_q}, \quad (26)$$

where the coupling constants $J_{i_1 \dots i_q}$ are extracted randomly from a Gaussian distribution, having vanishing mean-value and variance

$$\langle J_{i_1 \dots i_q}^2 \rangle \equiv \frac{J^2 (q-1)!}{(2n)^{q-1}}, \quad (27)$$

where J^2 is a constant which we set to be equal to one. The model has recently attracted a widespread attention from different communities, due to some peculiar features it enjoys. It has been shown that when $q \geq 4$ the model is highly chaotic [18, 19, 36, 37], although solvable in the large n limit [18, 19], thus creating a perfect situation to study relevant questions on quantum chaos which are usually out of reach for other chaotic models. Moreover, the SYK model has intriguing connections with the physics of black holes and quantum gravity, promoting itself as an ideal candidate to address new questions on holography and the AdS/CFT correspondence.

We will focus our attention to the SYK model with $q = 4$. A well-known feature of the model, which can be in principle a source of troubles for any eigensolver algorithm (both classical and quantum) whose goal is to reach the ground state, is that the density of states close to the ground energy level E_0 is rather high, *i.e.* the model has many excited states with energy parametrically close to E_0 . It particularly challenges the success of the VQE algorithm since separating the ground state from closely excited states becomes much harder.

As another characteristic, the SYK model is known to have two-fold degenerate eigenstates, if and only if $n = 4k + 2$ for any positive integer k [36, 37]. Denoting the two-fold degenerate ground states by $|\phi_1\rangle$ and $|\phi_2\rangle$, that we assume to be normalized and orthogonal to each other, the VQE target states for the SYK model are then given by all the possible linear combinations of the form:

$$|\phi_0\rangle = \frac{\alpha}{\sqrt{|\alpha|^2 + |\beta|^2}} |\phi_1\rangle + \frac{\beta}{\sqrt{|\alpha|^2 + |\beta|^2}} |\phi_2\rangle \quad (28)$$

with α and β being complex numbers. Therefore, the distance between the circuit state $|\psi(\boldsymbol{\theta})\rangle$ and the closest

state of the form $|\phi_0\rangle$ can be measured by computing

$$|\langle\psi(\boldsymbol{\theta})|\phi_1\rangle|^2 + |\langle\psi(\boldsymbol{\theta})|\phi_2\rangle|^2 \leq 1 \quad (29)$$

with the inequality which is saturated whenever $|\psi(\boldsymbol{\theta})\rangle$ takes exactly the form (28).

We will numerically show that the high-depth quantum circuit can effectively learn the ground state of the SYK model, thus showing that even complicated systems, involving non-local interactions and quantum chaos, can be universally studied through the VQE algorithm [1, 2].

2. Optimizing the Circuit

As with the Ising model, we start by checking if the SYK Hamiltonian (26) develops the barren plateau phenomenon with our layered circuit Ansatz (2). Assuming that at least one of $U_{\pm}(\boldsymbol{\theta}_{\pm})$ is a 2-design, let us examine if $\text{Var}_{\boldsymbol{\theta}}[\partial_k E(\boldsymbol{\theta})]$ with the SYK Hamiltonian is exponentially suppressed by computing $\text{Tr}(\mathcal{H}^2)$. The SYK Hamiltonian (26) has been exactly diagonalized up to $n = 15$. Moreover, an approximate analytical formula of the spectral density is at disposal in [38], which we use for testing the growth of $\text{Tr}(\mathcal{H}^2)$ with respect to the system size n . The results are presented in Figure 3. We clearly see, as in the Ising model, that $\text{Tr}(\mathcal{H}^2)$ scales like 2^n , which indicates the abundance of the barren plateaus in the VQE energy landscape of the SYK model.

The presence of the barren plateau phenomenon has also been tested numerically by computing the sample variance of $\partial_k E(\boldsymbol{\theta})$ over a random collection of 1000 parameters, as displayed in Figure 9a. It is evident that each component $\partial_k E(\boldsymbol{\theta})$ of the gradient is exponentially suppressed by increasing n [5, 12]. Interestingly, we see that for the SYK model, contrary to the case of the Ising, there is almost no transient regime, in which $\partial_k E(\boldsymbol{\theta})$ is large and decreasing by increasing the number of layers, a feature that is usually seen as a motivation to use shallow circuits in the VQE algorithms [12]. The lacking of the transient regime, which could be a consequence of the strongly chaotic nature [39] of the SYK Hamiltonian, would then constitute a clear obstacle to applying the VQE algorithm based on generic low-depth circuits.

On the other hand, as we can see from Figure 9b, the norm of the gradient vector is again increasing for the growing number L of layers, due to the saturation of the $\text{Var}_{\boldsymbol{\theta}}[\partial_k E(\boldsymbol{\theta})]$ with respect to L . The empirically measured growth rates between $\log \|\nabla_{\boldsymbol{\theta}} E(\boldsymbol{\theta})\|$ and $\log L$ are

n qubits	4	6	8	10
rate	0.503	0.503	0.501	0.502

matching the simple estimation formula (20). It tells that the gradient-based optimization can at least be initiated for high-depth quantum circuits, in the noiseless VQE setting, to replicate the ground state of the SYK model.

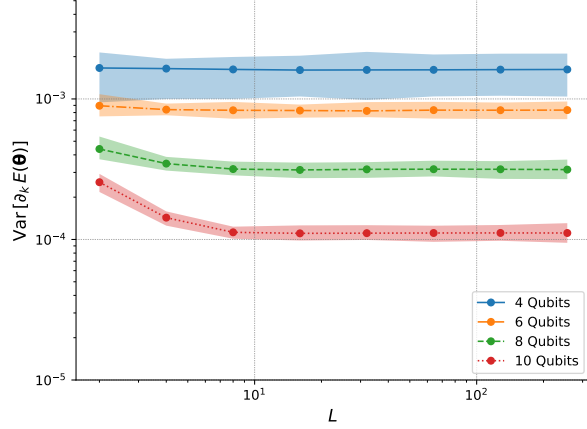
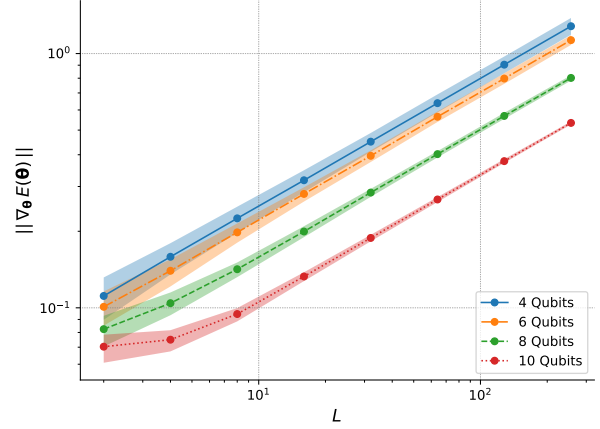
(a) Sample variance of the energy derivative $\partial_k E(\theta)$ (b) Sample average of the Euclidean norm of $\nabla_\theta E(\theta)$

FIG. 9. The barren plateau experiment for the SYK Hamiltonian (26). The shades indicate (a) the variance across gradient components $\{\partial_k E(\theta)\}_{k=1}^{nL}$, (b) the first and third sample quantiles.

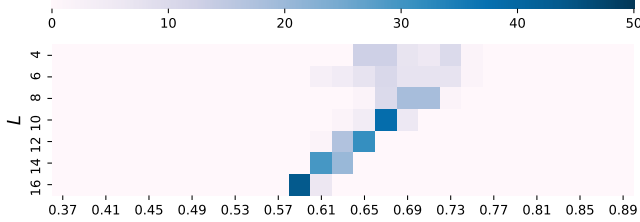


FIG. 10. Optimized VQE energy ($E(\theta^*) - E_0$) density for the SYK model over 35 distinct runs with random initialization.

As the next step, we examine the performance of the layered circuit Ansatz (2) in reaching the ground state of the SYK Hamiltonian, by repeating the same numerical experiments conducted in Section III 2 under the same choice of hyperparameters:

First, the density distribution of the optimized VQE energy $E(\theta^*)$ for randomly initialized *shallow* circuits of $4 \leq L \leq 16$ layers is illustrated in Figure 10, based on 35 sample VQE runs. One notable observation is the highly reduced spread of the final energy, compared to the Ising VQE energy distribution in Figure 5, even at very low depth. We interpret it as another manifestation of the fact that the required transition depth to an approximate 2-design is comparably low with the target Hamiltonian (26). Another – and perhaps the most important – point to stress is that, the mean value of the optimized VQE energy $E(\theta^*)$ decreases by stacking more layers, just like what has happened to the Ising VQE problem. It suggests that the high-depth circuits can reach a very good approximation of the SYK ground states.

Second, we have measured the performance of the layered circuit Ansatz (2) in approximating a ground state of the SYK model (26), as a function of the circuit depth. Specifically, the VQE single-run error $E(\theta^*) - E_0$ is drawn

in Figure 11. The high-depth circuit performs very well, reaching a zero error with the following accuracy,

$$|E(\theta) - E_0| \leq 10^{-5} \cdot \Delta E,$$

when the depth L arrives at the following values.

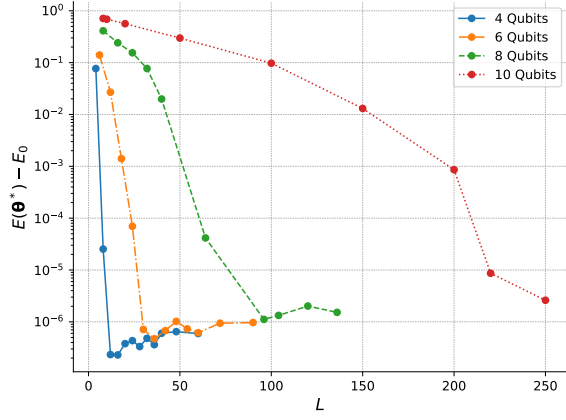
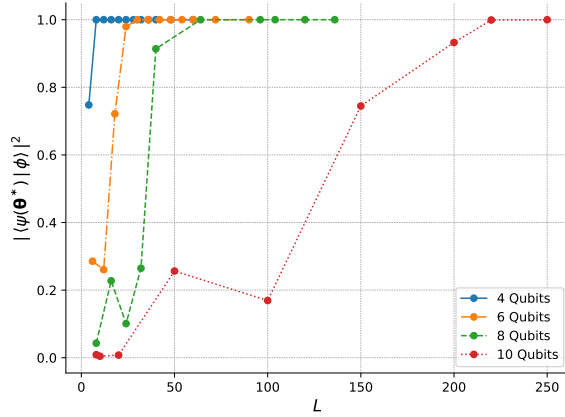
n qubits	4	6	8	10
L_v layers	12	30	96	220

We also note from Figure 11b that the fidelity between the optimized and ground states tends to decrease at an intermediate scale of depth, while the VQE error continues to reduce without temporary increase. Such contrasting behavior is due to the dense energy spectrum of the SYK model near the ground energy level E_0 . With an intermediate-depth circuit, the VQE algorithm is going to approximate not the exact ground states, but some low-lying excited states. In this way, the energy continues to decrease but the fidelity does not improve. However, for sufficiently deep circuits, the VQE algorithm can overcome the difficulty and reach an excellent agreement with the ground state.

Somewhat interestingly, we have seen that the necessary number L_v of layers to reach the high precision (21) is roughly in the same order, both for the SYK model and the Ising model. Moreover, the circuit (2) of $L \geq L_v$ reaches a high level of the parameteric expressibility, as shown in Figure 2. This compatibility highlights the universal effectiveness of the high-depth circuit in approximating *any* state in the Hilbert space, including *generic* random states as well as *non-generic* ground states.

V. DISCUSSION

We have examined certain aspects of the noiseless VQE optimization using the generic layered circuit Ansatz (2).

(a) The VQE optimization error $E(\theta^*) - E_0$ (b) Fidelity between the optimized and true ground states. As explained near (28)–(29), for the two-fold degenerate case $n = 4k + 2$, the sum $|\langle \psi(\theta^*) | \phi_1 \rangle|^2 + |\langle \psi(\theta^*) | \phi_2 \rangle|^2$ is drawn.FIG. 11. Single-run VQE outcomes for the SYK model (26) using the layered circuit Ansatz (2) at different depths L .

In particular, the high-depth circuit has been remarkably effective [4, 9] in simulating any random Haar states, as well as in solving the VQE problems defined for two quantum Hamiltonians, the Ising model and the SYK model, of distinct characteristics.

However, there are fundamental problems to the usage of high-depth circuits for the VQE problem on the near-term quantum devices [20]. Let us mention them here:

Firstly, to accurately estimate the gradient vector at randomly initialized parameters, it is necessary to sample the variational wavefunction $|\psi(\theta)\rangle$ exponentially many

times concerning the system size n , thereby invalidating the memory advantage of quantum devices. Such high demand is because the required number of sampling depends on the size of the gradient component, *i.e.*, $\mathcal{O}(1/\epsilon^\alpha)$ with $\epsilon = \min_{1 \leq k \leq nL} |\partial_k E(\theta)|$ that exponentially decays with n [5, 15]. We leave it as an interesting future problem to revisit the VQE optimization with noisy gradients, or even without direct gradient computation as in [40, 41], finding if the relatively simpler VQE landscape of the high-depth circuit can bring robust effectiveness against the sampling noise.

Secondly, and more severely, quantum hardware noise restricts our ability to implement the high-depth circuit state without decoherence, limiting the circuit depth of feasibility. Even aside from the decoherence, [42] has also demonstrated a noise-induced mechanism that causes the vanishing gradient phenomenon, which can be another barrier in applying the HQC algorithm to deep variational circuits. Various ongoing efforts on low-depth circuits, including to build up the efficient scheme for initialization [10, 11], optimization [14–16], and to implant some physical insights to circuit design [6–9, 12, 13] will become even more relevant in the noisy VQE problems. However, as it is clear from Figure 9, the SYK example shows that there exist cases of practical interest where the appearance of the barren plateaus cannot be mitigated by making use of low-depth circuits. It becomes then of primary interest to characterize which quantum Hamiltonians develop this obstacle.

One may note a certain degree of qualitative similarity between the VQE optimization trajectory of high-depth circuits, demonstrated in Section III 2, and the lazy learning [43] in over-parameterized neural networks. We speculate it as naturally emerging in any systems involving the high-dimensional parameter space. It would be very interesting to characterize why local extrema on the VQE landscape of the high-depth circuits can regularly reach a zero VQE error as if no bad local minima can exist [44].

ACKNOWLEDGMENTS

We thank Boris Hanin and Jae Yoo for helpful discussions. Joonho Kim acknowledges the support from the NSF grant PHY-1911298 and the Sivian fund. The work of DR is supported by the National Research Foundation of Korea (NRF) grant NRF-2020R1C1C1007591. Our Python code for the numerical experiments is written in JAX [45] and QuTip [46]. The experimental data are managed by using Weights & Biases [47].

[1] Alberto Peruzzo, Jarrod McClean, Peter Shadbolt, Man-Hong Yung, Xiao-Qi Zhou, Peter J. Love, Alán Aspuru-Guzik, and Jeremy L. O’Brien, “A variational eigenvalue solver on a photonic quantum processor,” *Nature Com-*

munications **5** (2014), 10.1038/ncomms5213, 1304.3061.
[2] Jarrod R McClean, Jonathan Romero, Ryan Babbush, and Alán Aspuru-Guzik, “The theory of variational hybrid quantum-classical algorithms,” *New Journal of*

- Physics **18** (2016), 10.1088/1367-2630/18/2/023023.
- [3] Yudong Cao, Jonathan Romero, Jonathan P. Olson, Matthias Degroote, Peter D. Johnson, Mria Kieferov, Ian D. Kivlichan, Tim Menke, Borja Peropadre, Nicolas P. D. Sawaya, and et al., “Quantum Chemistry in the Age of Quantum Computing,” *Chemical Reviews* **119**, 1085610915 (2019).
 - [4] Bobak Toussi Kiani, Seth Lloyd, and Reevu Maity, “Learning Unitaries by Gradient Descent,” (2020), [arXiv:2001.11897 \[quant-ph\]](#).
 - [5] Jarrod R. McClean, Sergio Boixo, Vadim N. Smelyanskiy, Ryan Babbush, and Hartmut Neven, “Barren plateaus in quantum neural network training landscapes,” *Nature Communications* **9** (2018), 10.1038/s41467-018-07090-4.
 - [6] Jin-Guo Liu, Yi-Hong Zhang, Yuan Wan, and Lei Wang, “Variational quantum eigensolver with fewer qubits,” *Physical Review Research* **1** (2019), 10.1103/physrevresearch.1.023025.
 - [7] Bryan T. Gard, Linghua Zhu, George S. Barron, Nicholas J. Mayhall, Sophia E. Economou, and Edwin Barnes, “Efficient symmetry-preserving state preparation circuits for the variational quantum eigensolver algorithm,” *npj Quantum Information* **6** (2020), 10.1038/s41534-019-0240-1.
 - [8] Kazuhiro Seki, Tomonori Shirakawa, and Seiji Yunoki, “Symmetry-adapted variational quantum eigensolver,” *Physical Review A* **101** (2020), 10.1103/physreva.101.052340.
 - [9] Roeland Wiersema, Cunlu Zhou, Yvette de Sereville, Juan Felipe Carrasquilla, Yong Baek Kim, and Henry Yuen, “Exploring entanglement and optimization within the Hamiltonian Variational Ansatz,” (2020), [arXiv:2008.02941 \[quant-ph\]](#).
 - [10] Edward Grant, Leonard Wossnig, Mateusz Ostaszewski, and Marcello Benedetti, “An initialization strategy for addressing barren plateaus in parametrized quantum circuits,” *Quantum* **3**, 214 (2019).
 - [11] Guillaume Verdon, Michael Broughton, Jarrod R. McClean, Kevin J. Sung, Ryan Babbush, Zhang Jiang, Hartmut Neven, and Masoud Mohseni, “Learning to learn with quantum neural networks via classical neural networks,” (2019), [arXiv:1907.05415 \[quant-ph\]](#).
 - [12] M. Cerezo, Akira Sone, Tyler Volkoff, Lukasz Cincio, and Patrick J. Coles, “Cost-Function-Dependent Barren Plateaus in Shallow Quantum Neural Networks,” (2020), [arXiv:2001.00550 \[quant-ph\]](#).
 - [13] Tyler Volkoff and Patrick J. Coles, “Large gradients via correlation in random parameterized quantum circuits,” (2020), [arXiv:2005.12200 \[quant-ph\]](#).
 - [14] James Stokes, Josh Izaac, Nathan Killoran, and Giuseppe Carleo, “Quantum Natural Gradient,” *Quantum* **4**, 269 (2020).
 - [15] Andrea Skolik, Jarrod R. McClean, Masoud Mohseni, Patrick van der Smagt, and Martin Leib, “Layer-wise learning for quantum neural networks,” (2020), [arXiv:2006.14904 \[quant-ph\]](#).
 - [16] Blint Koczor and Simon C. Benjamin, “Quantum Analytic Descent,” (2020), [arXiv:2008.13774 \[quant-ph\]](#).
 - [17] Subir Sachdev and Jinwu Ye, “Gapless spin-fluid ground state in a random quantum Heisenberg magnet,” *Physical Review Letters* **70**, 33393342 (1993).
 - [18] Alexei Kitaev, “A simple model of quantum holography,” <http://online.kitp.ucsb.edu/online/entangled15/kitaev/> & <http://online.kitp.ucsb.edu/online/entangled15/kitaev2/> (2015).
 - [19] Juan Maldacena and Douglas Stanford, “Remarks on the Sachdev-Ye-Kitaev model,” *Phys. Rev. D* **94**, 106002 (2016), [arXiv:1604.07818 \[hep-th\]](#).
 - [20] John Preskill, “Quantum Computing in the NISQ era and beyond,” *Quantum* **2**, 79 (2018).
 - [21] Andris Ambainis and Joseph Emerson, “Quantum t-designs: t-wise independence in the quantum world,” (2007), [arXiv:quant-ph/0701126 \[quant-ph\]](#).
 - [22] L. Welch, “Lower bounds on the maximum cross correlation of signals (Corresp.),” *IEEE Transactions on Information Theory* **20**, 397–399 (1974).
 - [23] A J Scott, “Optimizing quantum process tomography with unitary 2-designs,” *Journal of Physics A: Mathematical and Theoretical* **41**, 055308 (2008).
 - [24] Sukin Sim, Peter D. Johnson, and Aln AspuruGuzik, “Expressibility and Entangling Capability of Parameterized Quantum Circuits for Hybrid QuantumClassical Algorithms,” *Advanced Quantum Technologies* **2**, 1900070 (2019).
 - [25] Diederik P. Kingma and Jimmy Ba, “Adam: A Method for Stochastic Optimization,” (2017), [arXiv:1412.6980 \[cs.LG\]](#).
 - [26] Ashish Vaswani, Noam Shazeer, Niki Parmar, Jakob Uszkoreit, Llion Jones, Aidan N Gomez, Łukasz Kaiser, and Illia Polosukhin, “Attention is All you Need,” in *Advances in Neural Information Processing Systems 30*, edited by I. Guyon, U. V. Luxburg, S. Bengio, H. Wallach, R. Fergus, S. Vishwanathan, and R. Garnett (Curran Associates, Inc., 2017) pp. 5998–6008.
 - [27] J. Devlin, Ming-Wei Chang, Kenton Lee, and Kristina Toutanova, “BERT: Pre-training of Deep Bidirectional Transformers for Language Understanding,” in *NAACL-HLT* (2019).
 - [28] Christian Ledig, Lucas Theis, Ferenc Huszar, Jose Caballero, Andrew Cunningham, Alejandro Acosta, Andrew Aitken, Alykhan Tejani, Johannes Totz, Zehan Wang, and Wenzhe Shi, “Photo-Realistic Single Image Super-Resolution Using a Generative Adversarial Network,” in *Proceedings of the IEEE Conference on Computer Vision and Pattern Recognition (CVPR)* (2017).
 - [29] Thomas N. Kipf and Max Welling, “Semi-supervised classification with graph convolutional networks,” in *5th International Conference on Learning Representations, ICLR 2017, Toulon, France, April 24-26* (2017).
 - [30] Kouhei Nakaji and Naoki Yamamoto, “Expressibility of the alternating layered ansatz for quantum computation,” (2020), [arXiv:2005.12537 \[quant-ph\]](#).
 - [31] Subir Sachdev, *Quantum Phase Transitions*, 2nd ed. (Cambridge University Press, 2011).
 - [32] Zhongpeng Yang and Xiaoxia Feng, “A note on the trace inequality for products of Hermitian matrix power.” *JIPAM. Journal of Inequalities in Pure & Applied Mathematics [electronic only]* **3**, Paper No. 78, 12 p., electronic only—Paper No. 78, 12 p., electronic only (2002).
 - [33] Lei Wu, Zhanxing Zhu, and Weinan E, “Towards Understanding Generalization of Deep Learning: Perspective of Loss Landscapes,” (2017), [arXiv:1706.10239 \[cs.LG\]](#).
 - [34] Levent Sagun, Leon Bottou, and Yann LeCun, “Eigenvalues of the Hessian in Deep Learning: Singularity and Beyond,” (2017), [arXiv:1611.07476 \[cs.LG\]](#).
 - [35] Pratik Chaudhari, Anna Choromanska, Stefano Soatto, Yann LeCun, Carlo Baldassi, Christian Borgs, Jennifer Chayes, Levent Sagun, and Riccardo Zecchina,

- “Entropy-SGD: Biasing Gradient Descent Into Wide Valleys,” (2017), [arXiv:1611.01838 \[cs.LG\]](#).
- [36] Antonio M. García-García and Jacobus J. M. Verbaarschot, “Spectral and thermodynamic properties of the Sachdev-Ye-Kitaev model,” *Phys. Rev. D* **94**, 126010 (2016), [arXiv:1610.03816 \[hep-th\]](#).
 - [37] Jordan S. Cotler, Guy Gur-Ari, Masanori Hanada, Joseph Polchinski, Phil Saad, Stephen H. Shenker, Douglas Stanford, Alexandre Streicher, and Masaki Tezuka, “Black Holes and Random Matrices,” *JHEP* **05**, 118 (2017), [Erratum: *JHEP* 09, 002 (2018)], [arXiv:1611.04650 \[hep-th\]](#).
 - [38] Antonio M. García-García and Jacobus J. M. Verbaarschot, “Analytical Spectral Density of the Sachdev-Ye-Kitaev Model at finite N ,” *Phys. Rev. D* **96**, 066012 (2017), [arXiv:1701.06593 \[hep-th\]](#).
 - [39] Daniel A. Roberts and Beni Yoshida, “Chaos and complexity by design,” *Journal of High Energy Physics* **2017** (2017), 10.1007/jhep04(2017)121.
 - [40] Niru Maheswaranathan, Luke Metz, George Tucker, Dami Choi, and Jascha Sohl-Dickstein, “Guided evolutionary strategies: augmenting random search with surrogate gradients,” (PMLR, Long Beach, California, USA, 2019) pp. 4264–4273.
 - [41] Sean Welleck and Kyunghyun Cho, “MLE-guided parameter search for task loss minimization in neural sequence modeling,” (2020), [arXiv:2006.03158 \[cs.LG\]](#).
 - [42] Samson Wang, Enrico Fontana, M. Cerezo, Kunal Sharma, Akira Sone, Lukasz Cincio, and Patrick J. Coles, “Noise-Induced Barren Plateaus in Variational Quantum Algorithms,” (2020), [arXiv:2007.14384 \[quant-ph\]](#).
 - [43] Simon S. Du, Xiyu Zhai, Barnabas Póczos, and Aarti Singh, “Gradient Descent Provably Optimizes Over-parameterized Neural Networks,” (2019), [arXiv:1810.02054 \[cs.LG\]](#).
 - [44] Daniel Soudry and Yair Carmon, “No bad local minima: Data independent training error guarantees for multilayer neural networks,” (2016), [arXiv:1605.08361 \[stat.ML\]](#).
 - [45] James Bradbury, Roy Frostig, Peter Hawkins, Matthew James Johnson, Chris Leary, Dougal Maclaurin, and Skye Wanderman-Milne, “JAX: composable transformations of Python+NumPy programs,” (2018).
 - [46] J. R. Johansson, P. Nation, and F. Nori, “QuTiP 2: A Python framework for the dynamics of open quantum systems,” *Comput. Phys. Commun.* **184**, 1234–1240 (2013).
 - [47] Lukas Biewald, “Experiment Tracking with Weights and Biases,” (2020), software available from wandb.com.